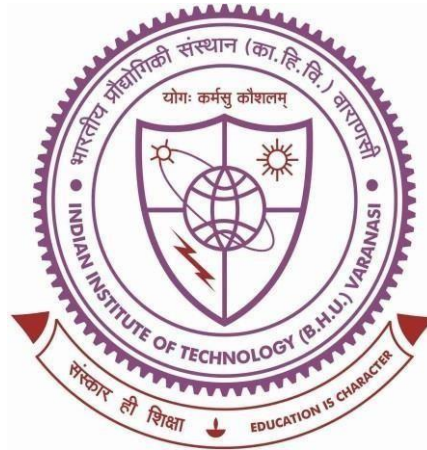


**Metamorphic evolution of granulite facies rocks of areas  
around Makrohar (Singrauli), Madhya Pradesh, India**



**Thesis submitted in partial fulfillment for the  
Award of Degree**

**Doctor of Philosophy**

**By**

**Vikas Pandey**

**DEPARTMENT OF CIVIL ENGINEERING  
INDIAN INSTITUTE OF TECHNOLOGY  
(BANARAS HINDU UNIVERSITY)  
VARANASI – 221005  
INDIA**

**Roll No. 17061011**

**2023**

*Dedicated to my beloved family  
and respected supervisor*

## CERTIFICATE

---

It is certified that the work contained in the thesis titled "*Metamorphic evolution of granulite facies rocks of areas around Makrohar (Singrauli), Madhya Pradesh, India*" by "*Vikas Pandey*" has been carried out under my supervision and that this work has not been submitted elsewhere for a degree.

It is further certified that the student has fulfilled all the requirements of Comprehensive Examination, Candidacy and SOTA for the award of Ph.D. Degree.



November, 2023

Prof. S.B Dwivedi  
( Supervisor)  
Engineering Geosciences Division  
Department of Civil Engineering  
Indian Institute of Technology (BHU)  
Varanasi, India  
Supervisor  
Department of Civil Engineering  
Indian Institute of Technology (BHU)  
Varanasi-221005

## DECLARATION BY THE CANDIDATE

I, **Vikas Pandey**, certify that the work embodied in this thesis is my own bonafide work and was carried out by me under the supervision of Prof. S.B Dwivedi from July 2017 to November 2023, at the Department of Civil Engineering, Indian Institute of Technology (BHU), Varanasi. The matter embodied in this thesis has not been submitted for the award of any other degree/diploma.

I declare that I have faithfully acknowledged and given credits to the research workers wherever their works have been cited in my work in this thesis. I further declare that I have not willfully copied any other's work, paragraphs, text, data, results, etc., reported in journals, books, magazines, reports, dissertations, theses, etc. or available at websites and have not included them in this thesis and have not cited as my own work.

Date: 14/12/2023

Place: Varanasi

*Vikas Pandey*

Signature of the Student

(Vikas Pandey)

## CERTIFICATE BY THE SUPERVISORS

It is certified that the above statement made by the student is correct to the best of my/our knowledge.

*S.B Dwivedi*  
14/12/23  
Prof. S.B Dwivedi (Supervisor)  
Engineering Geosciences Division  
Department of Civil Engineering  
Indian Institute of Technology (BHU)  
Varanasi

Supervisor  
Department of Civil Engineering  
Indian Institute of Technology, BHU  
Varanasi-221005

*S.B Dwivedi*  
14.12.23  
Head of Department  
Department of Civil Engineering  
Indian Institute of Technology (BHU)  
Varanasi  
जानपद अभियांत्रिकी विभाग  
Department of Civil Engineering  
भारतीय प्रौद्योगिकी संस्थान (बी.एच.यू.)  
Varanasi  
Indian Institute of Technology (BHU)  
Varanasi-221005

## COPYRIGHT TRANSFER CERTIFICATE

**Title of the Thesis:** “Metamorphic evolution of granulite facies rocks of areas around Makrohar (Singrauli), Madhya Pradesh, India”


**Name of the Student:** Mr. Vikas Pandey

### Copyright Transfer

The undersigned hereby assigns to the Indian Institute of Technology (Banaras Hindu University) Varanasi all rights under copyright that may exist in and for the above thesis submitted for the award of the “*Doctor of Philosophy*” degree.

Date: 14/12/2023

Place: Varanasi

  
Signature of the Student  
(Vikas Pandey)

**Note:** However, the author may reproduce or authorise others to reproduce material extracted verbatim from the thesis or derivative of the thesis for the author’s personal use, provided that the source and the Institute’s copyright notice are indicated.

## **ACKNOWLEDGEMENT**

---

---

I would like to express my deep sense of gratitude to my Supervisor Prof. S.B Dwivedi, Department of Civil Engineering, Indian Institute of Technology (Banaras Hindu University), Varanasi, for his valuable guidance, constant support and motivating comments throughout the completion of this research work. The countless discussions we had in his office and during fieldwork have played a pivotal role in shaping the evolution of my ideas. Having the opportunity to work under such a dedicated, enthusiastic, and passionate researcher, who genuinely cares for his students, has been an absolute privilege. Without his mentorship, completing this work would have been an insurmountable task.

Very special gratitude goes to Prof. S.S. Mandal (Head), Prof. P.K.S. Dikshit (Ex-Head), and Prof. P.K. Singh (Ex-Head), Department of Civil Engineering, IIT (BHU), for their support and making resources available to me. I would like to acknowledge the University Grants Commission (India) for providing financial support for the research work. I am also thankful to my RPEC members, Dr. Shishir Gour (internal expert) from the Department of Civil Engineering and Professor S.K Upadhyay (external expert) from the Department of Mathematics, at the Indian Institute of Technology (BHU), for their valuable suggestions throughout the work. I would also like to thank Dr. Medha Jha and Dr. B.N. Singh for helping me in several stances during my thesis work. I am also very thankful to Prof. S. P. Singh, Department of Geology, Bundelkhand University for their help in my research work. I represent my gratitude to Prof. N.V.C Rao, Department of Geology, B.H.U for facilitating the EPMA Laboratory. I am thankful to Dr. Gulab C. Gautam, Department of Geology, B.H.U for facilitating the Microscopy Laboratory.

I am also thankful to all technical staff, teaching, and non-teaching staff, especially Mr. Dinesh Singh and Mr. Akhilesh Kumar Jaiswar of the Department of Civil Engineering for their support during the research work. Finally, my sincere regards and thanks to those who have supported me one

way or the other during my entire Ph.D. period.

I want to express my gratitude to Dr. Raviranjana Kumar, Dr. Nikhilesh Singh, Mr. Manish Srivastava, Mr. Raviranjana Kumar Sharma, Mr. Sandeep Maddheshiya, and Dr. Pratigya Pathak for their unwavering assistance and support throughout my time in the lab. Working with all of you has been a delightful experience.

I owe a great debt of gratitude to my wife, Mrs. Shragdhara Pandey for her unwavering support during my academic journey, regardless of the challenges we faced. My parents, Mr. Vijay Shanker Pandey and Mrs. Gyanmati Pandey have consistently showered me with love and encouragement throughout my entire life. I am thankful to my younger brothers and sister for empowering me with strength and the support to pursue my aspirations and dreams.

I want to convey my never-ending appreciation to the Divine for the countless opportunities and blessings that have enriched my journey. Furthermore, there are a few more individuals with compassionate hearts who have played a role in my success, even though they may not be formally recognized. I extend my heartfelt thanks to each one of them.

Once more, I am deeply grateful to my supervisor and my family members, whose unwavering belief in me and continuous encouragement made this mission achievable.

Date: 14/12/2023

Vikas Pandey  
Research Scholar  
Engineering Geosciences Division  
Department of Civil Engineering  
Indian Institute of Technology (BHU)  
Varanasi- 221005, India



## LIST OF FIGURES

Figure No.	Titles	Page No.
<b>Figure 1.1</b>	(a) The arrangement of the worldwide collisional zones 2.0-1.8 billion years and accretionary belts formed between 1.8-1.3 Ga are shown on a configuration of the Columbia supercontinent. (b) Rodinia supercontinent reconstruction around 1000 Ma. The spot of the Chhotanagpur granite gneiss complex within India is shown by a red star. Proterozoic orogenic belts of the Indian subcontinent are marked by a black arrow- Central Indian Tectonic Zone and Eastern Ghat mobile belt.	2
<b>Figure 1.2</b>	Geological map of the Central Indian Tectonic Zone (CITZ) illustrates the arrangement of distinct lithological regions within the folded belt.	6
<b>Figure 3.1</b>	(a) The inset shows the Proterozoic mobile belts of India, including the CGGC. (b) Geological map of the Central granite gneiss complex and the study area is marked within the map.	26
<b>Figure 3.2</b>	Geological map of the Chhotanagpur Granite Gneiss Complex (CGGC) and Dalma Volcanic belt.	27
<b>Figure 3.3</b>	Geological map of the Makrohar area, Singrauli, Madhya Pradesh.	44
<b>Figure 3.4</b>	(a) Field photographs of migmatite from study area (b) Ptygmatic folding in granite gneiss (c) Agmatic structure in migmatite in Piprakurund area (d) stromatic structure in migmatite (e) Garnet porphyroblast in migmatite (f) Migmatite showing tight folding.	49
<b>Figure 3.5</b>	(a) Field photographs of pegmatite from study area (b) massive boulders of porphyritic granite (c) granite gneiss showing open fold and (d) granite gneiss showing folded fold (e) Contact of migmatite and pegmatite body (f) Interlayering of leucocratic migmatite and melanocratic amphibolite near Rehar river.	50
<b>Figure 3.6</b>	(a,b) Field image of gabbro and anorthosite as massive boulders (c) Dolerite as massive boulders (d) Close view of calc-silicate rock having garnet porphyroblasts (e) Calc- silicate granulite showing alteration and weathering (f) pegmatite vein in calc-silicate associated with amphibolite band.	52
<b>Figure 3.7</b>	(a) Field photographs of the amphibolite boulders from the Makorohar area (b) Field photographs of amphibolite exposure from the orgai area. (c) Field photographs of	54

<p>road cut section of mafic granulite from the study area. (d) Amphibolite occur as enclave in migmatite and overlain by weathered pegmatite. (e) Garnet porphyroblast in pelitic granulite (f) Amphibolite as an enclaves within pelitic granulite from the study area.</p>	
<p><b>Figure 4.1</b> (a) Outcrop photographs showing field features of the studied rock (b) Photomicrographs (PPL) image of porphyroblastic garnet showing zoning and corroded boundary. (c) Photomicrograph (PPL) showing inclusions of biotite and plagioclase within garnet porphyroblasts. (d) Photomicrograph (PPL) showing sillimanite needles occur in close vicinity with the garnet porphyroblast whereas quartz and biotite occur as inclusion phases within garnet. (e) Photomicrograph (PPL) showing that biotite, sillimanite needles and quartz occur as inclusion phase within garnet, whereas cordierite is present as groundmass. (f) Photomicrograph (PPL) showing sillimanite needles are wrapped around biotite flakes within the groundmass of cordierite and plagioclase and melt inclusion in ground mass.</p>	59
<p><b>Figure 4.2</b> (a) Megascopic hand specimen of garnet-bearing gneiss showing microfolding and garnet porphyroblast in quartzofeldspathic layer. (b) Photomicrographs (PPL) images showing biotite, plagioclase and quartz as inclusion in garnet porphyroblast. (c) Biotite is consumed to form garnet. (d) Garnet porphyroblasts in a matrix of biotite, quartz, and plagioclase. (e) Photomicrographs (XPL) images showing garnet porphyroblasts in a matrix of biotite, plagioclase and K-feldspar. (f) BSE image showing the inclusion of biotite and plagioclase in garnet porphyroblast.</p>	62
<p><b>Figure 4.3</b> (a) Mafic granulite exposed along with Pegmatite. (b) Field photograph of mafic granulite. (c) Photomicrograph shows clinopyroxene coexisting with orthopyroxene and has an inclusion of hornblende and quartz under PPL. (d) Photomicrograph shows inclusions of orthopyroxene, clinopyroxene and plagioclase in hornblende under PPL. (e) Photomicrograph shows the orthopyroxene, clinopyroxene and biotite occur as inclusion in hornblende coexisting with quartz and plagioclase. (f) Photomicrograph shows the biotite occurs as inclusion in clinopyroxene.</p>	66
<p><b>Figure 4.4</b> (a) Hand specimen of calc-silicate granulites showing alternate light and dark bands. (b) Photomicrograph shows garnet coexisting with cpx, plagioclase, and sphene under PPL. (c) Photomicrograph shows inclusions of</p>	68

	clinopyroxene and plagioclase in garnet under PPL. (d) & (e) Photomicrograph shows that garnet and sphene occur as inclusion in clinopyroxene coexisting with quartz and plagioclase. (f) Photomicrograph shows clinopyroxene rimming by garnet and plagioclase under PPL.	
<b>Figure 4.5</b>	(a) Field photographs of the garnetiferous amphibolite from the study area (b) Photomicrographs (PPL) shows clinopyroxene as inclusion within a massive form of garnet (c) Amphibole as in inclusion within the garnet porphyroblast. (d) Amphiboles are surrounded by a massive mass of clinopyroxene. (e) Inclusions of clinopyroxene, Biotite and ilmenite in garnet porphyroblast (f) Amphibole grains surrounded by clinopyroxene and plagioclase and biotite, ilmenite inclusion in garnet porphyroblast.	70
<b>Figure 4.6</b>	(a) Field photographs of the garnet absent amphibolite associated with felsic intrusion from the Makorohar area. (b) Photomicrographs (PPL) show clinopyroxene as inclusion within a massive form of amphibole. (c) Amphiboles show an octahedral to rhombohedral shape grains within the biotite laths. (d) Clinopyroxene is found in prismatic and lath-shaped textures, and associated with amphiboles. (e) Amphibole, clinopyroxene, and plagioclase are defining the foliation. (f) Amphiboles are surrounded by a massive mass of clinopyroxene.	73
<b>Figure 5.1</b>	The triangular diagram showing the variation in (spessartine + grossular)– almandine–pyrope end member compositions in the garnets from different rock types.	77
<b>Figure 5.2</b>	A $\text{CaSiO}_3$ - $\text{MgSiO}_3$ - $\text{FeSiO}_3$ composition diagram of pyroxenes showing the plot of clinopyroxenes and orthopyroxenes from different rock types.	80
<b>Figure 5.3</b>	Amphibole classification diagram (after Leake et al., 1965) for the amphibolite and mafic granulite of Makrohar granulite belt.	82
<b>Figure 5.4</b>	(a) A plot of microprobe analyses of biotites from different rock types in the Mg- Ti-(Fe+Mn) diagram. (b) A plot of microprobe analyses of biotites from different rock types in the Mg-(Al <sup>IV</sup> +Ti) - (Fe+Mn) diagram. (c) A plot of Ti vs Mg shows a negative trend. (d) A plot of $X_{\text{Fe}}/X_{\text{Mg}}$ vs $\text{TiO}_2$ shows a linear relationship.	85
<b>Figure 5.5</b>	Triangular $\text{NaAlSi}_3\text{O}_8$ - $\text{KAlSi}_3\text{O}_8$ - $\text{CaAl}_2\text{Si}_2\text{O}_8$ diagram showing plots of alkali feldspar and Plagioclase feldspar.	87
<b>Figure 5.6</b>	Back Scattered Electron (BSE) images are showing the microstructural and textural settings of monazite	92

	occurrences in the garnet-bearing gneiss and pelitic granulites of the study area. (a) BSE image of showing monazite inclusion in garnet of pelitic granulites. (b) Monazite grain occurs as an inclusion in cordierite as well as biotite. (c) Monazite occurs as inclusion in garnet of garnet-bearing gneisses. (d) Monazite occurs as inclusion in cordierite rim.	
<b>Figure 5.7</b>	BSE-SEM images of monazite grains of Pelitic granulites and garnet bearing gneisses.	94
<b>Figure 5.8</b>	(a) and (b) Weighted-average ages and probability density ages of pelitic granulite showing older age, (c) and (d) Weighted-average ages and probability density ages of pelitic granulite and garnet-bearing gneiss sample showing younger age.	95
<b>Figure 6.1</b>	(a) Total alkali versus silica (TAS) plot is used to classify metabasics (Le Maitre et al., 1989). (b) The Zr/Ti vs Nb/Y plot (Winchester and Floyd, 1977). (c) SiO <sub>2</sub> -FeO <sup>t</sup> MgO plot (Miyashiro, 1974). (d) Fet+Ti-Al-Mg ternary plot (Jensen, 1976).	125
<b>Figure 6.2</b>	(a) multi-element normalized spider diagram of metabasics (normalized after Sun and McDonough, 1989). (b) Chondrite normalized rare earth element plot (normalized after Anders and Grevesse 1989).	126
<b>Figure 6.3</b>	(a) Th/Nb vs Ba/Nb diagram (after Pearce and Stern, 2006) showing the influence of deep subduction component in the mantle source for the mafic granulites. (b) Nb/Th vs Zr/Nb diagram indicating the arc nature of the metabasics (after Sun and McDonough, 1989). (c) Zr vs Zr/Y diagram showing the island-arc nature of the metabasics (after Pearce and Norry, 1979). (d) Nb/Yb vs Th/Yb diagram (Pearce, 2008) depicting a subduction-related enrichment for the metabasic samples. Fields for intra-oceanic arc basalt and continental arcs are. (e) Ce/Nb vs Th/Nb plot (after Saunders et al., 1988) showing Island-arc affinity. (f) Y vs La/Nb diagram (modified after Floyd et al., 1991) showing back-arc affinity.	129
<b>Figure 7.1</b>	Coexisting Garnet-biotite pairs and derivative temperatures for different rocks.	142
<b>Figure 7.2</b>	Coexisting Garnet-biotite pairs and derivative pressures for different rocks.	143
<b>Figure 7.3</b>	Coexisting Garnet-Cordierite pairs and derivative temperatures for pelitic granulites.	143

<b>Figure 7.4</b>	Coexisting Garnet-Cordierite pairs and derivative pressures for pelitic granulites.	144
<b>Figure 7.5</b>	Coexisting Garnet-Clinopyroxene pairs and derivative temperatures for calc-silicate granulites.	145
<b>Figure 7.6</b>	Coexisting Garnet-Clinopyroxene pairs and derivative pressures for calc-silicate granulites.	145
<b>Figure 7.7</b>	Coexisting Orthopyroxene-Clinopyroxene pairs and derivative temperatures for mafic granulites.	146
<b>Figure 7.8</b>	Coexisting Orthopyroxene-Clinopyroxenes pairs and derivative pressures for mafic granulites.	147
<b>Figure 7.9</b>	Coexisting Garnet-clinopyroxene pairs and derivative temperatures for garnetiferous amphibolites.	149
<b>Figure 7.10</b>	Coexisting Garnet-clinopyroxene pairs and derivative pressures for garnetiferous amphibolites.	149
<b>Figure 7.11</b>	Coexisting Amphibole-plagioclase pairs and derivative temperatures for different rocks.	150
<b>Figure 7.12</b>	Coexisting Amphibole-plagioclase pairs and derivative pressures for different rocks.	150
<b>Figure 7.13</b>	T-X (H <sub>2</sub> O) Pseudosection calculated at fixed pressure 6 kbar, showing the effects of varying the molar proportions of bulk-rock H <sub>2</sub> O in pelitic granulites (sample K-1). The white dashed line shows the modelled composition of H <sub>2</sub> O (2.60 mol%).	161
<b>Figure 7.14</b>	P-T Pseudosection for pelitic granulite (sample K-1), showing the peak and post- peak metamorphic condition and isopleth of garnet, biotite and cordierite are contoured in the P-T pseudosection.	162
<b>Figure 7.15</b>	P-T pseudosection for mafic granulites (sample M-13), green shading is showing the equilibrium mineral assemblage (Opx-Cpx-Amp-Bt-Ilm) and blue shading represent peak metamorphic assemblage.	164
<b>Figure 7.16</b>	The T-XCO <sub>2</sub> pseudosection for calc-silicate granulite (M-7) from the study area was calculated in the NCFMAST-HC model system using the Perple_X software.	168
<b>Figure 7.17</b>	The T-X(H <sub>2</sub> O) pseudosection was computed at a constant pressure of 5.0 kbar, illustrating how changes in the molar proportions of H <sub>2</sub> O in garnetiferous amphibolites (sample S-9) impact the system. The black dashed line represents the modelled composition of H <sub>2</sub> O at 4.3 mol% and blue shading is showing the peak mineral assemblage.	168
<b>Figure 7.18</b>	A P-T pseudosection was constructed for garnetiferous	169

<p>amphibolites (sample S-9), revealing various metamorphic conditions including peak and post-peak stage.</p>	
<p><b>Figure 8.1</b> A diagram demonstrates (a) the progress of sedimentation and displays the pelitic granulites' protolith and (b) M1 metamorphic stage, found in patches within the granitic gneisses of CGGC (modified after Mukherjee et al. 2018; Yadav et al. 2020).</p>	<p>177</p>
<p><b>Figure 8.2</b> The P–T path has been constrained for Makrohar granulite belt, using three different rock types: pelitic granulites, mafic granulites and garnetiferous amphibolite, Where Pk: Peak P-T condition and Ppk: Post peak P-T condition.</p>	<p>181</p>

## LIST OF TABLES

Table No.	Titles	Page No.
<b>Table 3.1</b>	Generalised lithostratigraphic succession for the Proterozoic rocks of Makrohar area, (Solanki et al., 2003).	46
<b>Table 3.2</b>	Four metamorphic stages (M1 to M4) from Paleoproterozoic to Neoproterozoic with associated geochronology data from different areas of the CGGC (Modified after Sanyal and Sengupta 2012).	47
<b>Table 5.1</b>	Chemical analysis and structural formulae (based on 12 Oxygen) of garnet from pelitic granulites.	96-99
<b>Table 5.2</b>	Chemical analysis and structural formulae (based on 6 Oxygen) of Orthopyroxene from mafic granulites.	100
<b>Table 5.3</b>	Chemical analysis and structural formulae (based on 6 Oxygen) of Clinopyroxene from mafic granulite and amphibolites.	101-103
<b>Table 5.4</b>	Chemical analysis and structural formulae (based on 23 Oxygen) of amphibole from mafic granulite and amphibolites.	104-105
<b>Table 5.5</b>	Chemical analysis and structural formulae (based on 18 Oxygen) of Cordierite from pelitic granulites.	106
<b>Table 5.6</b>	Chemical analysis and structural formulae (based on 22 Oxygen) of biotite from pelitic granulites.	107-110
<b>Table 5.7</b>	Chemical analysis and structural formulae (based on 8 Oxygen) of Plagioclase from pelitic granulites and garnet bearing gneisses.	111-114
<b>Table 5.8</b>	Chemical analysis and structural formulae (based on 10 Oxygen) of Sillimanite from pelitic granulites.	115
<b>Table 5.9</b>	Chemical analysis and structural formulae (based on 5 Oxygen) of sphene from calc- silicate granulite (based on 12.5 Oxygen) of clinozoisite and (based on 3 Oxygen) of ilmenite from pelitic granulite, garnet- bearing gneiss and amphibolites.	116
<b>Table 5.10</b>	Representative electron microprobe analyses (EPMA), structural formula with their associated age of monazite grains (based on 4 Oxygens).	117-119
<b>Table 6.1</b>	Representative major oxides (in wt%), trace elements and REEs (in ppm) composition of metabasic.	130-131
<b>Table 7.1</b>	Results of P–T (pressure–temperature) estimation for pelitic granulites (K-1) and garnet bearing gneisses (M-1) from the	151

study area.	
<b>Table 7.2</b> Results of P–T (pressure–temperature) estimation for mafic granulite samples from the study area.	152
<b>Table 7.3</b> Results of P–T (pressure–temperature) estimation for calc-silicate granulites samples from the study area.	153
<b>Table 7.4</b> Results of P–T (pressure–temperature) estimation for garnetiferous amphibolite (S-9) and garnet absent amphibolite (S-14) samples from the study area.	154
<b>Table 7.5</b> Whole-rock data of pelitic granulite (K-1) from the study area.	160
<b>Table 7.6</b> Whole-rock data of mafic granulite (M-13) from the study area.	164
<b>Table 7.7</b> Whole-rock data of calc-silicate granulite (M-7) from the study area.	165
<b>Table 7.8</b> Whole-rock data of garnetiferous amphibolite (S-9) from the study area.	168

## **LIST OF ABBREVIATIONS**

---

---

<b>AX</b>	:	Activity-Composition
<b>BMB</b>	:	Bihar Mica Belt
<b>BSE</b>	:	Back Scattered image
<b>CGGC</b>	:	Chhotanagpur Granite Gneiss Complex
<b>CHIME</b>	:	CHemical Isochron MEmethod
<b>CIS</b>	:	Central Indian Shear Zone
<b>CITZ</b>	:	Central India Tectonic zone
<b>DOB</b>	:	Dalma Ophiolite Belt
<b>EDS</b>	:	Energy-dispersive X-ray spectrometry
<b>EPMA</b>	:	Electron microprobe analysis
<b>HFSE</b>	:	High field strength element
<b>HREE</b>	:	Heavy rare earth elements
<b>IBC</b>	:	Isobaric Cooling
<b>ICP-MS</b>	:	Inductively Coupled Plasma-Mass Spectrometry
<b>ITD</b>	:	Isothermal Decompression
<b>LA-ICP-MS</b>	:	Laser Ablation Inductively Coupled Plasma Mass Spectrometry
<b>LILE</b>	:	Large-ion lithophile element
<b>LREE</b>	:	Light rare earth element
<b>MMB</b>	:	Mahakoshal Mobile Belt
<b>NIB</b>	:	Northern Indian Block
<b>NSMB</b>	:	North Singhbhum Mobile Belt
<b>P-T</b>	:	Pressure and temperature
<b>P-T-t</b>	:	Pressure-Temperature-Time
<b>REE</b>	:	Rare earth element
<b>SEM</b>	:	Scanning electron microscope
<b>SIB</b>	:	Southern India Block
<b>SMB</b>	:	Sausar Mobile Belt

**SNNF** : Son Narmada North Fault  
**UHT** : Ultra high-temperature  
**XRF** : X-ray fluorescence

## LIST OF MINERAL ABBREVIATIONS

---

---

<b>Ab</b>	:	Albite
<b>Alm</b>	:	Almandine
<b>Amp</b>	:	Amphibole
<b>Ann</b>	:	Annite
<b>An</b>	:	Anorthite
<b>Ap</b>	:	Apatite
<b>Aug</b>	:	Augite
<b>Bt</b>	:	Biotite
<b>Chl</b>	:	Chlorite
<b>Cpx</b>	:	Clinopyroxene
<b>Crd</b>	:	Cordierite
<b>Di</b>	:	Diopside
<b>Grs</b>	:	Grossular
<b>Grt</b>	:	Garnet
<b>Gr</b>	:	Graphite
<b>Hbl</b>	:	Hornblende
<b>Ilm</b>	:	Ilmenite
<b>Kfs</b>	:	K-feldspar
<b>Ky</b>	:	Kyanite
<b>Liq</b>	:	Liquid
<b>Mag</b>	:	Magnetite
<b>Ml</b>	:	Melt
<b>Mnz</b>	:	Monazite
<b>Opx</b>	:	Orthopyroxene
<b>Pl</b>	:	Plagioclase
<b>Py</b>	:	Pyrope
<b>Qz</b>	:	Quartz
<b>Sil</b>	:	Sillimanite

**Sps** : Spessartine  
**Ts** : Tschermakite  
**Zrn** : Zircon

## PREFACE

---

---

The Chhotanagpur Granite Gneiss Complex (CGGC) is a region of high-grade metamorphic basement with metasedimentary enclaves and mafic to ultramafic rocks. It covers about 100,000 km<sup>2</sup> and is located at the eastern extension of the Central India Tectonic Zone (CITZ). The CGGC terrain is bounded in the north by the Mahakoshal Mobile Belt and in the south by the North Singhbhum Mobile Belt (NSMB). The most prominent rock types within the CGGC are granitic gneisses, migmatites, and amphibolites. The Monghyr-Saharsa Ridge and the South Purulia Shear Zone are bounded at the northern and southern periphery of the CGGC, respectively. Chhotanagpur Granite Gneiss Complex CGGC consists of granite gneisses and migmatites with enclaves of metasedimentary and metaigneous rocks. The study area around Makrohar lies in the northwestern extremity of Chhotanagpur Granite Gneiss Complex (CGGC) and occurs as a tongue parallel to the Son Narmada South Lineament. The Makrohar granulite belt comprises high-grade metamorphic rocks including pelitic granulites, mafic granulites, calc-silicate granulite, amphibolites, garnet-bearing gneisses, dolerite, and metabasalt are exposed as major rock types.

Microscopic investigations of the studied rock samples have revealed distinct types of mineral assemblages in five rock types such as: Garnet-cordierite-biotite-sillimanite- plagioclase-ilmenite-quartz in pelitic granulites; garnet-biotite-plagioclase-ilmenite -quartz- k-feldspar in garnet-bearing gneisses; orthopyroxene-clinopyroxene-amphibole-plagioclase- biotite-quartz-ilmenite in mafic granulites; garnet- clinopyroxene-plagioclase-sphene-quartz- clinozoisite in calc-silicate granulites and garnet- clinopyroxene-amphibole-plagioclase- biotite-quartz-ilmenite in amphibolites. Electron microprobe analyses (EPMA) of minerals from the different mineral assemblages are used to observe the characteristics of mineral phases. Garnet compositions range between 24.35 and 84.86 mol% almandine, 0.34 to 17.93

mol% pyrope, 3.17 to 73.25 mol% grossularite, and 1.97 to 3.98 mol% spessartite. Garnet  $X_{Mg}$  in different rock types varies from 0.01 to 0.28, exhibiting trends: garnetiferous amphibolite > garnet-bearing gneisses > pelitic granulites > calc-silicate granulites. Cordierite shows  $X_{Mg}$  ranging from 0.63 to 0.66, with traces of  $Na_2O$  (0.46–0.89 wt%) and  $K_2O$  (0.04–

0.16 wt%). Biotite  $X_{Mg}$  varies widely (0.30–0.69) influenced by Ti and  $Al^{VI}$  occupancy in the octahedron, with a notable decrease in  $X_{Mg}$  as Ti increases.  $X_{Mg}$  of amphiboles vary from

0.38 to 0.71, while amphibole's  $Al^{IV}$  and  $Al^{VI}$  content vary (0.32–1.45 and 0.13–0.60 p.f.u., respectively). Analyzed pyroxenes plot on a  $CaSiO_3$ - $MgSiO_3$ - $FeSiO_3$  diagram, with orthopyroxene close to hypersthene and coexisting clinopyroxene within the diopside and augite field in mafic granulites, and the hedenbergite field in calc-silicate granulites. Orthopyroxene and clinopyroxene  $X_{Mg}$  range between 0.44–0.49 and 0.29–0.70, respectively, with relatively lower  $Al_2O_3$  content (0.32–0.69 wt%) in the investigated areas compared to other terrains.

EPMA monazite dating has delineated two distinct age ranges for monazite: 1529 to 1743 Ma and 874 to 1111 Ma from pelitic granulites, while garnet-bearing gneiss preserves ages from 822 to 1014 Ma. Weighted mean age distributions obtained using the ISOPLOT program (Figure 5.8a–d) depict a metamorphic peak at an estimated  $1655 \pm 30$  Ma ( $n = 14$ , MSWD = 4.3) and a retrograde metamorphism at  $910 \pm 31$  Ma ( $n = 19$ , MSWD = 9.3). Geochemical examination of metabasics show significant variation in major oxide composition. The Zr/Ti vs Nb/Y diagram places garnetiferous amphibolites in the sub-alkaline basalt category and mafic granulites in the basaltic-andesite field, signifying characteristics of both spreading and subduction tectonics. Analysis of immobile trace elements suggests minimal contamination from the Earth's crust in the formation of these rocks. Discrimination diagrams (Th/Nb vs Ba/Nb, Nb/Th vs Zr/Nb) suggest metabasics associated with arc-like settings,

aligning with subduction influences. These samples resemble intra-oceanic arc basalt and arc basalt fields, indicating their formation in active island arc margins related to subduction during orogenic events. Evidence suggests their formation during subduction and arc-related settings, contributing to Neoproterozoic collisional tectonism. These metabasic patches underwent metamorphism before and during peak conditions and interacted with fluids derived from subduction, resulting in geochemical alterations. Retrograde metamorphic processes occurred during their exhumation.

Multiple classic geothermobarometry techniques, like garnet–biotite and garnet–cordierite thermometers, were used to gauge temperature and pressure in pelitic granulites (Grt-Crd-Bt-Sil-Pl-Qz). For instance, in pelitic granulites, Gt-Bt thermometry suggested prograde temperatures around  $690 \pm 62$  °C at a consistent pressure of 6 kbar. Meanwhile, the garnet-biotite-plagioclase-quartz geobarometer (GBPQ) indicated pressures of 6.2 kbar at 600°C. In garnet-bearing gneisses, Gt-Bt thermometry indicated temperatures of  $566 \pm 33$  °C at 6 kbar, while GBPQ suggested 5.11 kbar at 600°C. Similarly, Grt-Crd thermometry displayed post-peak temperatures of  $575 \pm 28$  °C at 5 kbar, whereas garnet-cordierite-sillimanite-quartz geobarometry showed pressures of  $5.55 \pm 0.73$  kbar at 600°C. Overall, the average conditions involving garnet, biotite, plagioclase, cordierite, and sillimanite were around  $679 \pm 63$  °C/ $5.3 \pm 0.9$  kbar considering  $(H_2O) = 1$ . For calc-silicate granulites, conventional garnet–clinopyroxene exchange geothermometers and garnet–clinopyroxene–plagioclase–quartz geobarometers determined temperature and pressure conditions. Garnet–clinopyroxene exchange thermometry indicated temperatures of  $675 \pm 89$  °C at 7 kbar pressure. The average conditions with garnet, clinopyroxene, plagioclase, epidote, and quartz were approximately  $624 \pm 97$  °C/ $5.6 \pm 0.8$  kbar assuming  $(H_2O) = 1$ . Mafic granulite pressure-temperature conditions were evaluated using orthopyroxene–clinopyroxene conventional exchange geothermobarometers. Peak temperatures were around  $887 \pm 62$  °C at 6 kbar, and peak stage pressures

were estimated at  $6.15 \pm 0.3$  kbar. Post-peak metamorphic stage pressures, derived from the aluminium-in-amphibole barometer, were estimated at  $2.28 \pm 0.15$  kbar. For garnetiferous amphibolites, garnet–clinopyroxene conventional geothermobarometers determined peak temperatures at approximately  $643 \pm 51$  °C at 5.0 kbar pressure. Post-peak metamorphic stage pressures were estimated at  $4.30 \pm 0.28$  kbar for garnetiferous amphibolites and  $5.26 \pm 0.21$  kbar for garnet-absent amphibolites. In the study, P–T pseudosections were computed for various granulite types using different chemical systems. The pelitic granulite displayed equilibrium, peak, and retrograde mineral assemblages at distinct temperature and pressure ranges. Similarly, the mafic granulite exhibited mineral assemblages across varying P–T conditions. Isobaric T–X (CO<sub>2</sub>) pseudosections for calc-silicate granulites constrained CO<sub>2</sub> mole fractions and temperature conditions for specific mineral assemblages. Garnetiferous amphibolites were also analyzed, showing distinct metamorphic stages marked by specific mineral compositions at different P–T conditions. The peak metamorphic stage was characterized by higher P–T settings, while the post-peak stage had different mineral compositions at lower P–T conditions, as delineated by amphibole and biotite isopleths. Overall, various traditional geothermobarometry methods were employed to estimate temperature and pressure conditions for different rock types, providing insights into their metamorphic histories and mineral assemblage stability ranges at different stages. Three thermodynamic approaches were employed to establish temperature and pressure (P–T) conditions: traditional geothermobarometry, multi-equilibrium geothermometry, and forward modeling. Across garnet-bearing gneisses, granulites, and amphibolites in the study area, these methods produced similar results. The P–T–t paths delineate a rocks journey through P–

T space over time. In the case of pelitic granulites, thermodynamic calculations and pseudosection modeling revealed a clockwise P-T-t path. At the peak stage, the rock underwent burial, evident in temperature shifts indicating increased pressure. This phase witnessed high-pressure conditions, ranging from 7.40 to 6.70 kbar, and temperatures between 760 to 740°C. Subsequently, the rock followed an almost isothermal decompression path (ITD) into the post-peak stage, characterized by garnet and cordierite, at pressures of 4.80 to 4.60 kbar and temperatures from 730 to 725°C. Similar clockwise P-T-t paths were identified in garnetiferous amphibolites. At the peak stage, the rock exhibited a mineral assemblage stable at 7.3–7.1 kbar/810–790°C. Post-peak conditions showcased different minerals at 4.5–4.1 kbar/610–590°C due to decompression, indicating exhumation. Mafic granulites in the Makrohar area also displayed a clockwise P-T path. Peak temperatures were recorded at  $887^{\circ} \pm 62^{\circ}\text{C}$  at 6 kbar, while post-peak conditions were estimated at  $2.28 \pm 0.15$  kbar/ $593 \pm 50^{\circ}\text{C}$ . Two distinct metamorphic events were identified from the Paleoproterozoic to Neoproterozoic periods, delineating the complex evolution of the CGGC terrain. Monazite dating revealed two ages for the pelitic protolith at ~1655 Ma and ~910 Ma, with only pelitic granulites preserving the peak metamorphic event (M1) during Late Paleoproterozoic (~1655 Ma) and exhumation resulted into retrograde metamorphism during Neoproterozoic (~910 Ma) era. Several magmatic intrusions documented in the CGGC indicated a diverse geological history involving subduction and collision-related tectonic processes. The geodynamic interpretation of the study area suggests interactions between Archean cratons, rift development, sedimentation, and subduction-related tectonics. The CGGC metamorphic events offer insights into crustal thickening, and subduction processes, shaping

the region geological history during the Paleoproterozoic era and exhumation during Neoproterozoic era. These findings align with the formation of supercontinents and various orogenic events, contributing to a broader understanding of continental movements and geological changes across different geological eras.